Coastal vulnerability across the Pacific dominated by El Niño/Southern Oscillation

Citation	Barnard, P. L., Short, A. D., Harley, M. D., Splinter, K. D., Vitousek, S., Turner, I. L., ... & Heathfield, D. K. (2015). Coastal vulnerability across the Pacific dominated by El Niño/Southern Oscillation. Nature Geoscience, 8(10), 801-807. doi:10.1038/NGEO2539
DOI	10.1038/NGEO2539
Publisher	Nature Publishing Group
Version	Version of Record
Terms of Use	http://cdss.library.oregonstate.edu/sa-termsofuse

nature geoscience

ARTICLES

PUBLISHED ONLINE: 21 SEPTEMBER 2015 | DOI: 10.1038/NGEO2539

Coastal vulnerability across the Pacific dominated by El Niño/Southern Oscillation

Patrick L. Barnard[1]*, Andrew D. Short[2], Mitchell D. Harley[3,4], Kristen D. Splinter[4], Sean Vitousek[1], Ian L. Turner[4], Jonathan Allan[5], Masayuki Banno[6], Karin R. Bryan[7], André Doria[8], Jeff E. Hansen[9], Shigeru Kato[10], Yoshiaki Kuriyama[6], Evan Randall-Goodwin[1,11], Peter Ruggiero[12], Ian J. Walker[13] and Derek K. Heathfield[13]

To predict future coastal hazards, it is important to quantify any links between climate drivers and spatial patterns of coastal change. However, most studies of future coastal vulnerability do not account for the dynamic components of coastal water levels during storms, notably wave-driven processes, storm surges and seasonal water level anomalies, although these components can add metres to water levels during extreme events. Here we synthesize multi-decadal, co-located data assimilated between 1979 and 2012 that describe wave climate, local water levels and coastal change for 48 beaches throughout the Pacific Ocean basin. We find that observed coastal erosion across the Pacific varies most closely with El Niño/Southern Oscillation, with a smaller influence from the Southern Annular Mode and the Pacific North American pattern. In the northern and southern Pacific Ocean, regional wave and water level anomalies are significantly correlated to a suite of climate indices, particularly during boreal winter; conditions in the northeast Pacific Ocean are often opposite to those in the western and southern Pacific. We conclude that, if projections for an increasing frequency of extreme El Niño and La Niña events over the twenty-first century are confirmed, then populated regions on opposite sides of the Pacific Ocean basin could be alternately exposed to extreme coastal erosion and flooding, independent of sea-level rise.

Upper-end sea-level rise scenarios could displace up to 187 million people by the end of the twenty-first century[1], with flood losses exceeding US$1 trillion per year for the world's major coastal cities by 2050 (ref. 2). However, prior studies typically omit key oceanographic components of water level elevations during storms that drive severe beach erosion and flooding of coastal communities, and can be highly temporally and spatially variable. As the climate system evolves nonlinearly, so too will the spatial distribution of mean and extreme wind speed, wave height, period and direction, water level anomalies, and resulting coastal response, as is evident from trends observed over the past two decades[3].

Here we investigate the potential of coherent, anomalous patterns of physical forcing and coastal response across the Pacific Ocean through a unique synthesis of multi-decadal coastal change data sets compiled from over 650 years of surveys of 48 open-coast beaches representing the majority of the low-lying, vulnerable population centres. Further, we explore the relationship between regional wave energy flux, wave direction and water level anomalies, and basin-wide and global climatological patterns through common climate indices. Establishing a direct link between climate variability, via key indices, and coastal change will not only support adaptation efforts for agencies and coastal communities preparing for the uncertain future impacts of climate change, but also provide the basis for short-term, emergency management planning.

Twelve climate indices were analysed to represent Pacific Ocean basin-wide and regional climate variability and atmospheric forcing (for example, atmospheric pressure, wind) that, in turn, drive oceanographic processes (for example, waves, storm surge) and lead to enhanced exposure to coastal hazards. Based on strong correlations among many indices (Supplementary Fig. 1 and Supplementary Table 1), four representative indices are identified that characterize the observed spatial and temporal variability of the Pacific Ocean basin climate: the Pacific Decadal Oscillation (PDO), Multivariate ENSO Index (MEI), Southern Annular Mode (SAM) and Pacific North American (PNA). PDO is a multi-decadal pattern of climate variability affecting the Pacific Ocean, with the warm phase (positive PDO index values) characterized by higher sea surface temperature (SST) in the northeast and tropical Pacific Ocean and lower sea-level pressure (SLP) in the central north Pacific region[4]. Superimposed on PDO is the related, but less temporally persistent El Niño/Southern Oscillation (ENSO), which describes the interannual variability in SST, SLP and atmospheric forcing across the equatorial Pacific, with implications for global

[1]United States Geological Survey, Pacific Coastal and Marine Science Center, Santa Cruz, California 95060, USA. [2]University of Sydney School of Geosciences, Sydney, New South Wales 2006, Australia. [3]University of Ferrara, Department of Physics and Earth Sciences, Via Saragat 1, 44122 Ferrara, Italy. [4]UNSW Australia, Water Research Laboratory, School of Civil and Environmental Engineering, Sydney, New South Wales 2093, Australia. [5]Oregon Department of Geology and Mineral Industries, Coastal Field Office, Newport, Oregon 97365, USA. [6]Port and Airport Research Institute, Nagase 3-1-1, Yokosuka, Kanagawa 239-0826, Japan. [7]University of Waikato, Private Bag 3105, Hamilton 3240, New Zealand. [8]Scripps Institution of Oceanography, University of California, San Diego, La Jolla, California 92093, USA. [9]University of Western Australia, School of Earth and Environment, 35 Stirling Highway, Crawley, Western Australia 6009, Australia. [10]Toyohashi University of Technology, Aichi 441-8580, Japan. [11]University of California, Santa Cruz, Department of Ocean Sciences, Santa Cruz, California 95060, USA. [12]Oregon State University, College of Earth, Ocean, and Atmospheric Sciences, Corvallis, Oregon 97331, USA. [13]University of Victoria, Coastal Erosion and Dune Dynamics (CEDD) Laboratory, Department of Geography, Victoria, British Columbia V8P 5C2, Canada. *e-mail: pbarnard@usgs.gov

Table 1 | Summary of shoreline, wave and water level anomalies.

Region	+MEI El Niño	−MEI La Niña	PDO	SAM	PNA
Shoreline erosion anomaly (%)					
California	129*	13	N/A	14	182*
Pacific Northwest	50*	126*	−20*	28	88*
Central Pacific	67*	58	N/A	1	67*
Japan	−18	−17*	43*	−15*	25*
Australia	−62	94*	8	30*	−96
New Zealand	−75	−33	−60	13	−18
Wave energy flux anomaly (%)					
California	32*	−6*	7*	9*	33*
Pacific Northwest	18*	6*	−1	18*	15*
Central Pacific	18*	−10*	0*	−1*	19*
Japan	−5	−6	−20*	−8*	−8
Australia	−12*	27*	−9*	28*	−16*
New Zealand	−12*	13*	−5	12*	−10*
Wave direction anomaly (deg)					
California	−4*	6*	−3*	3*	−5*
Pacific Northwest	−8*	4*	−4*	1	−8*
Central Pacific	−6*	13*	−4*	5*	−7*
Japan	−6	−2	23	9	11*
Australia	−2	0	4*	2	−1
New Zealand	8	−4	−3*	−2	5
Water level anomaly (m)					
California	0.11*	−0.06*	0.01	−0.04*	0.08*
Pacific Northwest	0.12*	−0.04*	−0.01	0.01	0.10*
Central Pacific	−0.01*	0.00	−0.03*	−0.02*	−0.02*
Japan	0.00	0.01	0.02	0.02	0.03*
Australia	−0.04*	0.01*	−0.07*	0.00	−0.04*
New Zealand	N/A	N/A	N/A	N/A	N/A

Summary of the regionally averaged anomalies for annual shoreline erosion (Fig. 2), and winter (DJF) wave energy flux (Fig. 3a), wave direction (Fig. 3b) and water level (Fig. 4) for the top five winter index events for MEI (El Niño), PDO, SAM and PNA, and the bottom five winter index events for MEI (La Niña). *Complete study site agreement within the region. See Supplementary Table 3 for data of all indices and from the individual study sites.

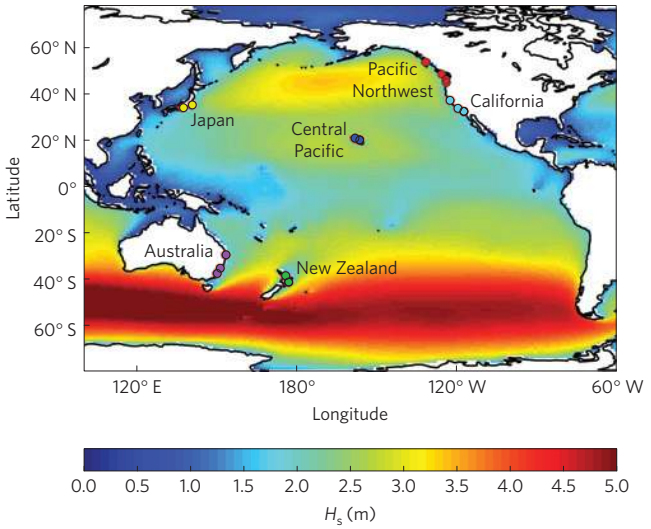

Figure 1 | Study site locations. Locations of the 16 study sites (grouped into six regions) within the Pacific Ocean basin where co-located wave, water level and shoreline change data were analysed. Mean significant wave heights from 1996 to 2005 are shown[39].

climate[5]. ENSO is characterized by multiple indices, with MEI representing a comprehensive assessment of conditions in the tropical Pacific Ocean[6]. The El Niño (La Niña) phase corresponds to positive MEI values (negative MEI values) with lower (higher) SLP and higher (lower) SST in the eastern equatorial Pacific. For the Southern Hemisphere, SAM represents SLP and wind patterns in the mid- and high latitudes[7]. Negative phases of SAM are related to northerly shifts in storm tracks that directly impact the southern extremities of Australia and New Zealand, with more storm generation in the Southern Ocean during positive phases[8]. Influenced by ENSO, PNA is an indication of extra-tropical variability and atmospheric circulation patterns over the North Pacific Ocean, with the positive mode associated with a stronger jet stream and increased storminess in the mid-latitudes[9].

Regionally coherent patterns of both forcing (represented by key climate indices) and response (represented by measured shoreline changes) have been observed along discrete sections of the Pacific Ocean margin. For example, El Niño events are linked to elevated wave energy and shoreline retreat in Japan during the boreal fall[10]. The combined effects of elevated wave energy, water levels and directional shifts common during El Niño events have historically resulted in severe coastal erosion along the North American west coast in boreal winter, best documented during the 1982–1983, 1997–1998 and 2009–2010 events[11–16]. By contrast, in New Zealand, beaches have been shown to rapidly erode during La Niña, owing to the more frequent passage of extra-tropical cyclones, and gradually recover during El Niño periods[17]. Rotational shifts in embayed beach orientation along the southeast coast of Australia coincide with phase shifts of ENSO, where wave heights generally increase and become more easterly during La Niña phases[18,19]. Higher rates of coastal erosion along the southeastern coastline of Australia have also been linked to La Niña, when warmer water in the western Pacific leads to increased cyclonic activity, wave heights and sea-surface elevations[20–23]. SAM is significantly correlated to both significant wave height and directional variability for large portions of the South Pacific Ocean[8]. Although climate variability is clearly a dominant driver in these localized studies, regional patterns of atmospheric forcing and oceanographic/coastal response have been investigated piecemeal, and therefore the possibility of broader, Pacific Ocean basin-scale relationships have not been established.

Regional patterns of coastal vulnerability

Wave height, period and directional data from the ECMWF ERA-Interim global wave reanalysis data set[24] and water level data from 14 tide gauges, spanning from 1979 to 2012, were compiled for 16 study sites and assimilated into six regions within the Pacific Ocean basin (Fig. 1, see Supplementary Fig. 2 for regional monthly wave statistics). The wave and water level data were compared against co-located shoreline change data sets with at least semi-annual survey frequency for five consecutive years during this time frame. A total of $n = 48$ shoreline data sets were identified meeting this criteria, reaching up to 40 years in duration, within each of the six regions: New Zealand ($n = 7$); Australia ($n = 14$); Japan ($n = 4$); Central Pacific (Hawaii, USA, $n = 9$); Pacific Northwest (British Columbia, Canada and Washington/Oregon, USA, $n = 8$) and California, USA ($n = 6$; Supplementary Table 2). In the Northern Hemisphere, the wave-height response to teleconnection patterns is the strongest in boreal winter (December–January–February [DJF]), when atmospheric pressure is most variable, but also tends to be stronger in the eastern Pacific[25], where land has a minimal influence on local wind and wave fields[26]. Across all regions for this study, the strongest, most coherent seasonal signals of forcing and response are observed in boreal winter, hence our focus here. First, we will discuss the dominant patterns of intra-annual coastal change for the Pacific Ocean regions in relation to climate variability, followed by

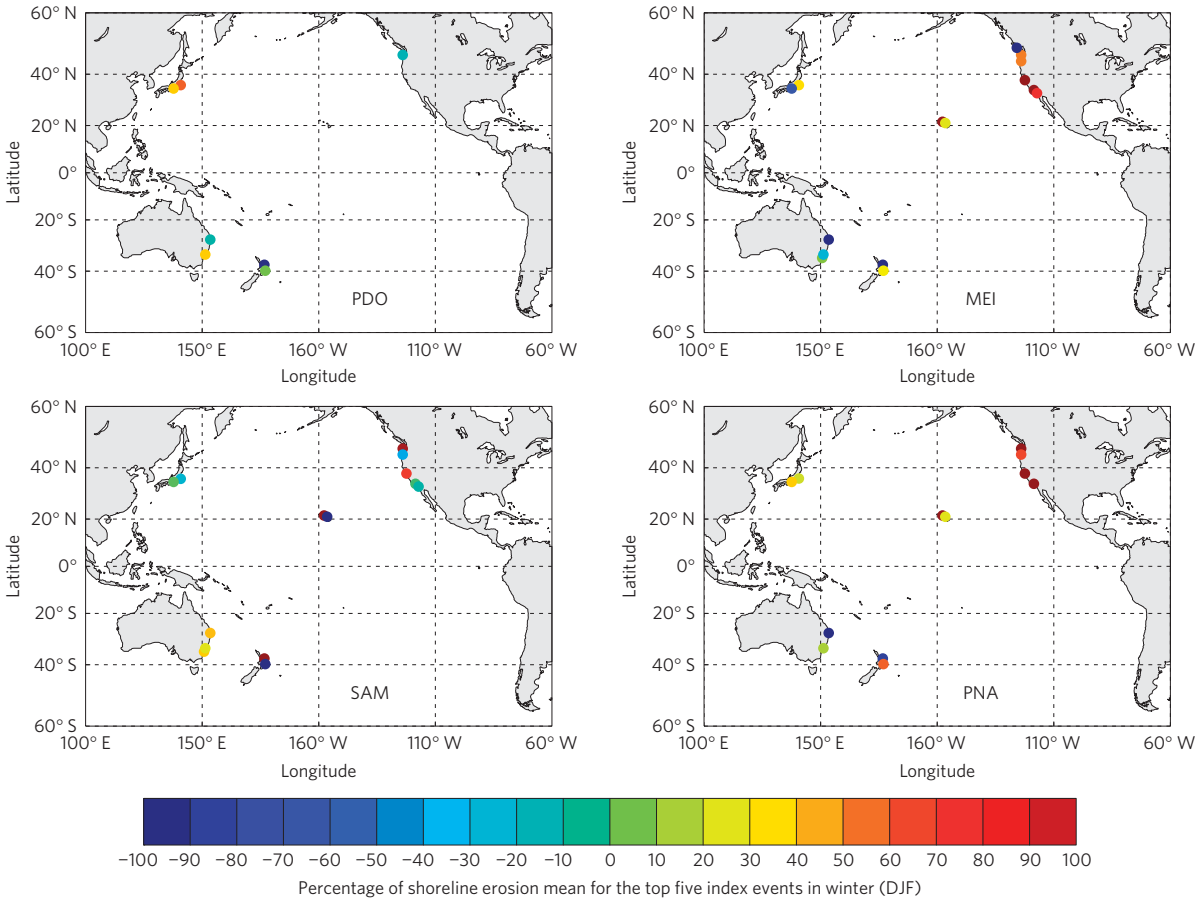

Figure 2 | Shoreline erosion anomalies. Annual shoreline erosion for the top five climate index events, relative to the mean, during winter (DJF) from 1979 to 2012 (see Supplementary Fig. 3 for annual/DJF time periods for all 12 indices).

the physical drivers: wave energy flux (a function of wave height and period (Methods)), wave direction and water levels.

The relationships between broad-scale atmospheric forcing, regional oceanographic conditions, and coastal response can be established by examining the extremes of climate variability in the Pacific Ocean basin in more detail. As a proxy for anomalous coastal erosion, the minimum annual shoreline position (most landward) for the largest winter climate index events was computed relative to the mean annual minimum position of each shoreline change record (Methods, Table 1 and Fig. 2, see Supplementary Fig. 3 for annual climate index events). During the five largest winter El Niño events (strongly positive MEI) from 1979 to 2012, the northeast Pacific (that is, Central Pacific, California, and Pacific Northwest) and northern Japan regions eroded 69% more than during typical winters, with the largest erosion recorded in California, tapering into the Pacific Northwest, whereas erosion was 68% less for the southern Pacific (that is, New Zealand and Australia) and southern Japan. For the top five winter La Niña events (strongly negative MEI), Australia and the Pacific Northwest experienced severe erosion, 110% above normal, but no strong or consistent signal for the other regions. The winter positive PDO erosion signal shows a less distinct, but broadly similar pattern to El Niño in the western Pacific (that is, Japan, Australia and New Zealand), with elevated erosion in Japan and suppressed erosion in the southern Pacific. The strongest five winter SAM events are linked to moderately more erosion for the southern Pacific regions, and slightly less for Japan, with mixed results for other regions. The highest five winter PNA events show a strong, consistent erosion anomaly in the northeast Pacific and Japan, similar to El Niño, with the strongest signal in California, but no clear pattern in the southern Pacific.

As a key driver of elevated coastal erosion, wave energy flux was substantially above normal (+23%) during the five largest winter El Niño events in the northeast Pacific, but collectively suppressed (−9%) for the western Pacific (Table 1 and Fig. 3a). Conversely, during the five largest La Niña events, the southern Pacific regions experienced elevated winter wave energy flux, and although the Pacific Northwest was moderately elevated, the more southerly regions in the northeast Pacific were suppressed. The extreme PDO events show similar spatial patterns but reduced wave energy anomalies relative to ENSO, but with a particularly strong oscillatory signal across the Northern Hemisphere for negative PDO events, ranging from +21% in Japan to −16% in the northeast Pacific. During the most positive winter SAM events, wave energy flux was higher in the southern Pacific, but also the North American west coast. The positive PNA relationship with wave energy flux shows a consistent and strong signal similar to El Niño in winter.

Of the wave metrics investigated, wave direction shows the strongest relationships, with indices spanning multiple seasons. Although climate-driven clockwise or anticlockwise rotations existed across large geographic regions, the most notable shift was in the northeast Pacific (Table 1 and Fig. 3b). For example, during the top five winter index events, every region in the northeast Pacific experienced anticlockwise (southerly) wave direction shifts for PDO (−4°), El Niño (−6°) and PNA (−7°), and clockwise (northerly) shifts for La Niña (+8°). These consistent rotation patterns in mean wave direction are generally opposed in the western Pacific regions.

Water level anomalies follow a pattern consistent with the relationships found for mean wave direction, with the strongest signal along the North American west coast, mostly restricted to

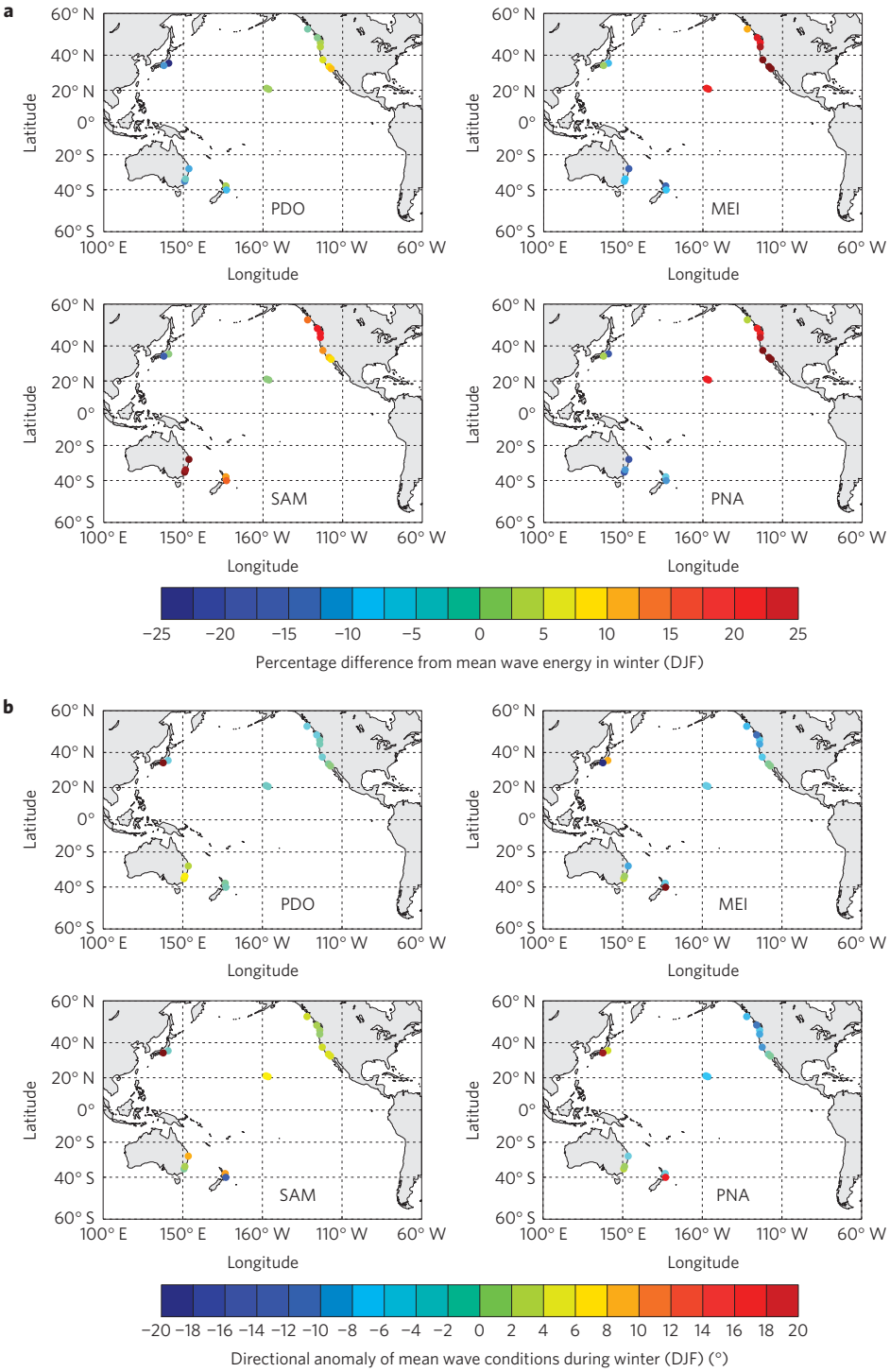

Figure 3 | Wave energy flux and direction anomalies. Divergence from the mean for the top five climate index events during winter (DJF) from 1979 to 2012. **a**, Wave energy flux. **b**, Wave direction. (See Supplementary Figs 4 and 5 for annual/DJF time periods and mean/upper 5% values for all 12 indices.)

winter, and with a more moderate pattern across the rest of the Pacific Ocean basin (Table 1 and Fig. 4). During the five largest El Niño events, winter water levels averaged 0.11 m higher for the North American west coast, varying only slightly across the approximately 2,500 km of coastline from southern California, USA, to British Columbia, Canada. Conversely, mean winter water level anomalies in the central Pacific and western Pacific were insignificant or suppressed, at least partly owing to their location in the basin relative to the direction of Coriolis deflection. For the largest La Niña events, slightly elevated water levels are observed in winter for the western Pacific, whereas the North American west coast regions are suppressed. The winter water level patterns of extreme PNA events are similar to El Niño for the North American west coast. In most cases, the physical forcing patterns discussed above are similar for the upper 5% and annual metrics, although the latter is muted (Supplementary Figs 4–6 and Supplementary Table 3).

Climate indices that reflect basin-wide atmospheric conditions are significantly correlated (P-values ≤ 0.05) with wave conditions throughout the Pacific Ocean, particularly during boreal winter and, in some cases, boreal spring (March–April–May [MAM]) and

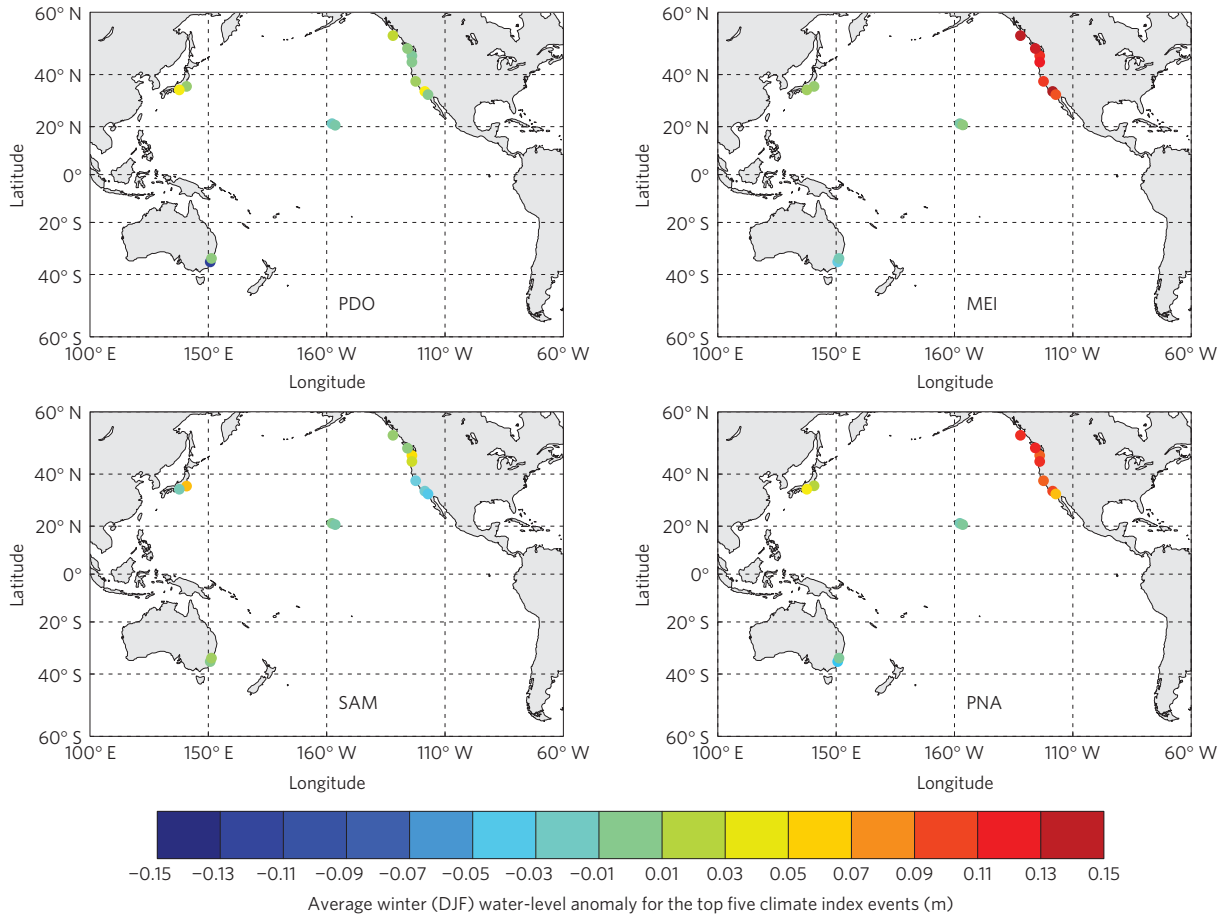

Figure 4 | Water level anomalies. Average water level anomalies for the top five climate index events during winter (DJF) from 1979 to 2012. (See Supplementary Fig. 6 for annual/DJF time periods for all 12 indices.)

fall (September–October–November [SON]). For example, MEI shows a statistically significant positive correlation with winter mean and upper 5% wave energy flux for all sites in the Central Pacific and California, and a significant negative correlation for mean winter wave direction across the northeast Pacific (Fig. 5). Although a positive correlation exists with MEI and wave energy flux in Japan for summer (June–July–August [JJA]) and fall, in comparison to the northeast Pacific, regions along the western Pacific margin show an opposing relationship between MEI and wave energy flux and direction for winter and spring. Similar latitudinal and east–west oscillatory relationships for seasonal wave conditions are also apparent across the Pacific Ocean basin for other indices, albeit with more sub-regional variability (for example, PDO, SAM) or regional restriction (for example, PNA), following other studies[25] (see Supplementary Fig. 7 and Supplementary Table 4 for all 12 climate index-wave correlation analyses).

Synthesis of climate variability and coastal response

The world's coastlines will respond to global climate changes and the associated adjustment of oceanographic forcing. This study has established strong, statistically significant relationships between wave energy flux, wave direction, water level anomalies, and key climate indices representing both Pacific Ocean basin-wide and regional atmospheric conditions. The relationship between atmospheric forcing and coastal change for some Pacific regions is less distinct, indicating stronger, unresolved local influences (for example, tropical storm paths, nearshore hydrodynamics, sediment supply, coastal orientation, exposure, morphology, and so on), or weakened by the temporal resolution (typically monthly or greater) and limited length (as few as five years) of the shoreline data sets. Nevertheless, links between climate indices and anomalously high coastal erosion are evident across the entire Pacific Ocean basin, with the strongest relationships related to the ENSO endmembers, El Niño (positive MEI) and La Niña (negative MEI), which manifest in unique combinations of oceanographic forcing and coastal erosion. For example, strong wave directional shifts and elevated wave energy flux, water levels, and coastal erosion characterize boreal winter El Niño conditions along the North American west coast, whereas the Central Pacific exhibits identical patterns except for the water level anomaly. The greater wave energy flux during El Niño events not only leads to anomalously high erosion in the northeast Pacific, but the more southerly wave directions also drive acute erosion at the southern ends of littoral cells throughout the North American west coast[12,15]. Southeastern Australia and the Pacific Northwest experience increased erosion rates during La Niña with increased wave energy flux, but only minor changes in wave direction and water level. Although more variable seasonally and/or sub-regionally, Japan and New Zealand also exhibit significant relationships with ENSO forcing and coastal response. These relationships establish a physical link between ENSO variability, atmospheric forcing, wave energy flux, directional shifts and coastal response in both the eastern and western Pacific Ocean, which had been hypothesized in earlier studies[11,23].

Implications for future coastal hazards

With these patterns established and given future climate change projections, we can identify changes to atmospheric forcing, the oceanographic hazards they drive, and coastal regions around the

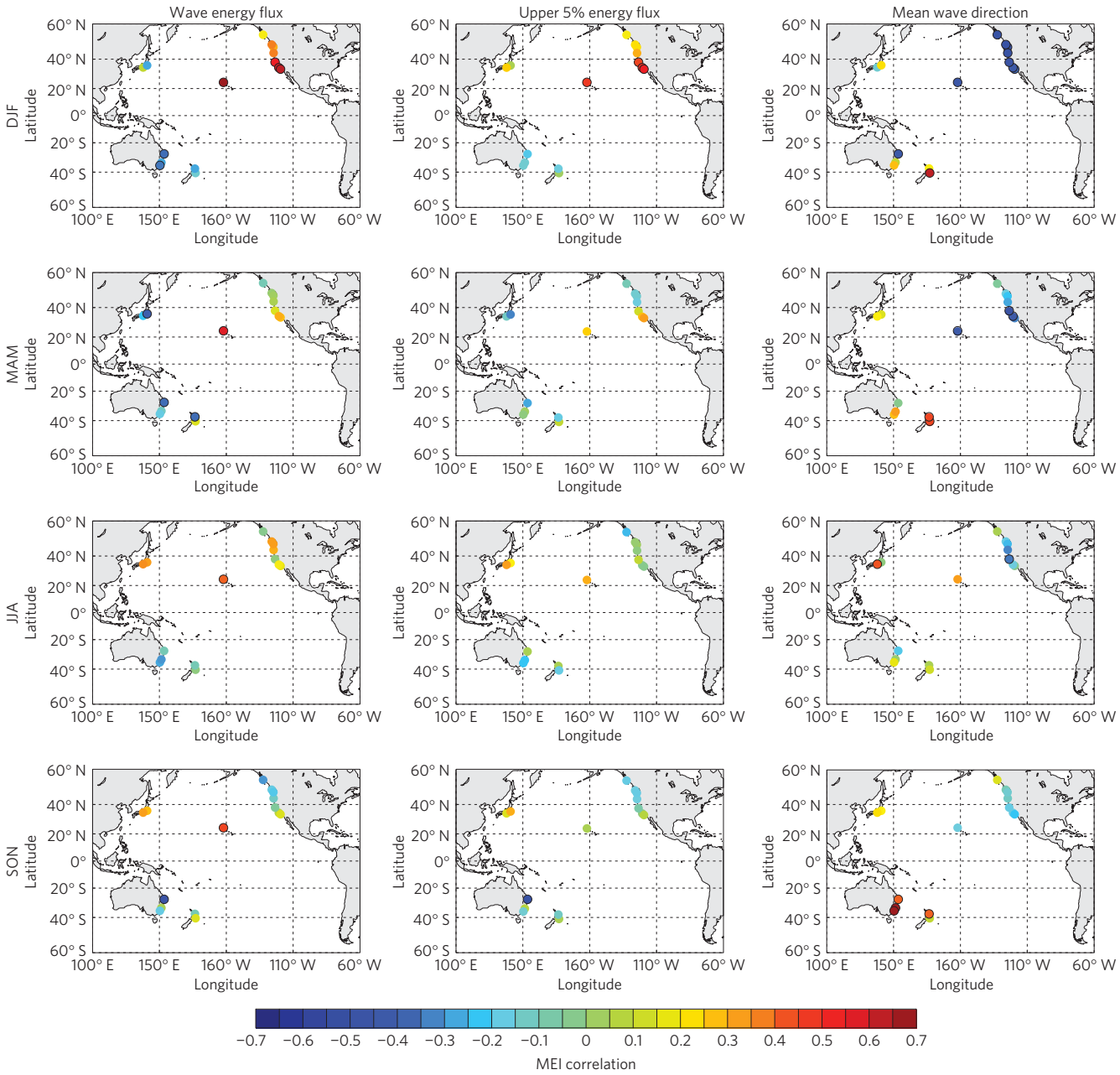

Figure 5 | Wave metrics and MEI correlations. Correlation (R) between MEI and wave energy flux, upper 5% energy flux, and direction from sites across the Pacific Ocean basin for boreal winter (DJF), spring (MAM), summer (JJA) and fall (SON). Black outlines indicate significant correlations above the 95% confidence interval. (see Supplementary Fig. 7 for plots of all 12 indices).

Pacific Rim that are more likely to be exposed to these changes. Although projections vary markedly, one area of consensus among global climate models is an increase in wind strength, wave period, and thus wave energy generated in the Southern Ocean for the twenty-first century[27–30]. These trends are related to the SAM continuing to move towards its more positive polarity, representing poleward shifts of Southern Hemisphere storm tracks, acceleration in the westerly jet, increased wind waves in the region, and northward propagating swell into the Pacific Ocean basin, consistent with Hadley cell expansion in both hemispheres[8,31,32]. On the basis of our study, an increase in the SAM would result in elevated wave energy and more severe intra-annual erosion in southeastern Australia and New Zealand, as well as higher wave energy for the northeast Pacific.

Projections of the future occurrence and magnitude of El Niño events for the twenty-first century are less certain[33], ranging from no distinguishable changes[34] to a possible doubling of extreme events[35]. Our study demonstrates that El Niño events result in wave directional shifts, elevated wave energy and severe coastal erosion for the Central Pacific and California, and moderate erosion in the Pacific Northwest. Using an ensemble of 21 Global Climate Models (GCMS) from the Coupled Model Intercomparison Project Phase 5 (CMIP5; ref. 36), a recent study predicted a 73% increase in the frequency of extreme La Niña events associated with global warming during the twenty-first century, with the majority of these La Niñas following an extreme El Niño event[37]. Also, a present trend towards a stronger La Niña-like Walker circulation was statistically linked to increases in global mean temperature[38]. This study and prior work suggests that, for the southern Pacific regions, an increase in La Niña conditions will result in elevated wave energy and more extensive coastal erosion. If these trends of increasing La Niña

strength and frequency are realized, the elevated wave conditions and associated coastal erosion noted in this study for southeastern Australia and the Pacific Northwest, as well as sub-regionally for New Zealand, may continue. Further, if the projections materialize for a noticeable increase in the frequency of both extreme El Niño and La Niña events[37], then populated regions on opposite sides of the Pacific Ocean basin will be alternately exposed to extreme coastal erosion and flooding, independent of sea-level rise.

Methods

Methods and any associated references are available in the online version of the paper.

Received 29 June 2015; accepted 17 August 2015; published online 21 September 2015

References

1. Nicholls, R. J. *et al.* Sea-level rise and its possible impacts given a 'beyond 4 °C world' in the twenty-first century. *Phil. Trans. R. Soc. A* **369,** 161–181 (2011).
2. Hallegate, S., Green, C., Nicholls, R. J. & Corfee-Morlot, J. Future flood losses in major coastal cities. *Nature Clim. Change* **3,** 802–806 (2013).
3. Young, I. R., Zieger, S. & Babanin, A. V. Global trends in wind speed and wave height. *Science* **332,** 451–455 (2011).
4. Mantua, N. J., Hare, S. R., Zhang, Y., Wallace, J. M. & Francis, R. C. A Pacific decadal climate oscillation with impacts on salmon. *Bull. Am. Meteorol. Soc.* **78,** 1069–1079 (1997).
5. Wolter, K. The Southern Oscillation in surface circulation and climate over the tropical Atlantic, Eastern Pacific, and Indian Oceans as captured by cluster analysis. *J. Clim. Appl. Meteorol.* **26,** 540–558 (1987).
6. Wolter, K. & Timlin, M. S. in *Proc. 17th Clim. Diagnostics Work.* 52–57 (CIMMS and the School of Meteorology, Univ. of Oklahoma, 1993).
7. Rogers, J. C. & van Loon, H. Spatial variability of sea level pressure and 500 mb height anomalies over the Southern Hemisphere. *Mon. Weath. Rev.* **110,** 1375–1392 (1982).
8. Hemer, M. A., Church, J. A. & Hunter, J. R. Variability and trends in the directional wave climate of the Southern Hemisphere. *Int. J. Climatol.* **30,** 475–491 (2010).
9. Wallace, J. M. & Gutzler, D. S. Teleconnections in the geopotential height field during the Northern Hemisphere. *Mon. Weath. Rev.* **109,** 784–812 (1981).
10. Kuriyama, Y., Banno, M. & Suzuki, T. Linkages among interannual variations of shoreline, wave and climate at Hasaki, Japan. *Geophys. Res. Lett.* **39,** L06604 (2012).
11. Storlazzi, C. D. & Griggs, G. B. Influence of El Niño-Southern Oscillation (ENSO) events on the evolution of central California's shoreline. *Geol. Soc. Am. Bull.* **112,** 236–249 (2000).
12. Sallenger, A. H. *et al.* Sea-cliff erosion as a function of beach changes and extreme wave runup during the 1997–1998 El Niño. *Mar. Geol.* **187,** 279–297 (2002).
13. Allan, J. C. & Komar, P. D. Climate controls on US West Coast erosion processes. *J. Coast. Res.* **22,** 511–529 (2006).
14. Abyswirigunawardena, D. S. & Walker, I. J. Sea level responses to climate variability and change in northern British Columbia. *Atmosphere* **46,** 277–296 (2008).
15. Barnard, P. L. *et al.* The impact of the 2009–10 El Niño Modoki on U.S. West Coast beaches. *Geophys. Res. Lett.* **38,** L13604 (2011).
16. Heathfield, D. K., Walker, I. J. & Atkinson, D. E. Erosive water level regime and climatic variability forcing of beach–dune systems on south-western Vancouver Island, British Columbia, Canada. *Earth Surf. Land.* **38,** 751–762 (2013).
17. Smith, R. K. & Benson, A. P. Beach profile monitoring: How frequent is sufficient? *J. Coast. Res.* **34,** 573–579 (2001).
18. Ranasinghe, R., McLoughlin, R., Short, A. & Symonds, G. The Southern Oscillation Index, wave climate, and beach rotation. *Mar. Geol.* **204,** 273–287 (2004).
19. Harley, M. D., Turner, I. L., Short, A. D. & Ranasinghe, R. Interannual variability and controls of the Sydney wave climate. *Int. J. Climatol.* **30,** 1322–1335 (2010).
20. Thom, B. G. in *Landform Evolution in Australia: Canberra* (eds Davies, J. L. & Williams, M. A.) 197–214 (Australian National University Press, 1978).
21. Bryant, E. Regional sea level, Southern Oscillation and beach change, New South Wales, Australia. *Nature* **305,** 213–216 (1983).
22. Clarke, D. J. & Eliot, I. G. Low-frequency variation in the seasonal intensity of coastal weather systems and sediment movement on the beachface of a sandy beach. *Mar. Geol.* **79,** 23–39 (1988).
23. Phinn, S. R. & Hastings, P. A. Southern Oscillation influences on the wave climate of south-eastern Australia. *J. Coast. Res.* **8,** 579–592 (1992).
24. Dee, D. P. *et al.* The ERA-Interim reanalysis: Configuration and performance of the data assimilation system. *Q. J. R. Meteorol. Soc.* **137,** 553–597 (2010).
25. Shimura, T., Mori, N. & Mase, H. Ocean waves and teleconnection patterns in the Northern Hemisphere. *J. Clim.* **26,** 8654–8670 (2013).
26. Tokinaga, H. & Xie, S.-P. Wave- and anemometer-based sea surface wind (WASWind) for climate change analysis. *J. Clim.* **24,** 267–285 (2011).
27. Mori, N., Yasuda, T., Mase, H., Tom, T. & Oku, Y. Projections of extreme wave climate change under global warming. *Hydrol. Res. Lett.* **4,** 15–19 (2010).
28. Dobrynin, M., Murawsky, J. & Yang, S. Evolution of the global wind wave climate in CMIP5 experiments. *Geophys. Res. Lett.* **39,** L18606 (2012).
29. Hemer, M. A., Fan, Y., Mori, N., Semedo, A. & Wang, X. L. Projected changes in wave climate from a multi-model ensemble. *Nature Clim. Change* **3,** 471–476 (2013).
30. Semedo, A. *et al.* Projection of global wave climate change toward the end of the twenty-first century. *J. Clim.* **26,** 8269–8288 (2013).
31. Previdi, M. & Liepert, B. G. Annular modes of Hadley cell expansion under global warming. *Geophys. Res. Lett.* **34,** L22701 (2007).
32. Arblaster, J. M., Meehl, G. A. & Karoly, D. J. Future climate change in the Southern Hemisphere. Competing effects of ozone and greenhouse gases. *Geophys. Res. Lett.* **38,** L02701 (2011).
33. Collins, M. *et al.* The impact of global warming on the tropical Pacific Ocean and El Niño. *Nature Geosci.* **3,** 391–397 (2010).
34. Stevenson, S. L. Significant changes to ENSO strength and impacts in the twenty-first century: Results from CMIP5. *Geophys. Res. Lett.* **39,** L17703 (2012).
35. Cai, W. *et al.* Increasing frequency of extreme El Niño events due to greenhouse warming. *Nature Clim. Change* **4,** 111–116 (2014).
36. WCRP Coupled Model Intercomparison Project Phase 5—CMIP5. *CLIVAR Exchanges* **16** (Special issue), 1–52 (2011).
37. Cai, W. *et al.* Increased frequency of La Niña events under greenhouse warming. *Nature Clim. Change* **5,** 132–137 (2015).
38. L'Heureux, M. L., Lee, S. & Lyon, B. Recent multidecadal strengthening of the Walker Circulation across the tropical Pacific. *Nature Clim. Change* **3,** 571–576 (2013).
39. Erikson, L. H., Hegermiller, C. A., Barnard, P. L., Ruggiero, P. & van Ormondt, M. Projected wave conditions in the Eastern North Pacific under the influence of two CMIP5 climate scenarios. *Ocean Model.* (2015).

Acknowledgements

Funding for this project was provided by the Coastal and Marine Geology Program of the United States Geological Survey. California beach survey data collection was funded by the California Department of Boating and Waterways and the United States Army Corps of Engineers. Many thanks to C. Fletcher, A. Gibbs and B. Richmond for providing beach survey data from Hawaii. Waikato Regional Council and Hawkes Bay Regional Council provided the New Zealand data. Australian survey data collection in New South Wales was supported by the Australian Research Council and Warringah Council, with Queensland data provided by Gold Coast City Council. Wave and water level data for these sites was supplied by Manly Hydraulics Laboratory (New South Wales) and Gold Coast City Council (Queensland).

Author contributions

P.L.B. and A.D.S. developed the original concept for this study. P.L.B. directed the analysis and wrote the original version of this paper. M.D.H., S.V. and E.R.-G., analysed the data. All authors contributed to interpreting results and improvement of this paper.

Additional information

Supplementary information is available in the online version of the paper. Reprints and permissions information is available online at www.nature.com/reprints. Correspondence and requests for materials should be addressed to P.L.B.

Competing financial interests

The authors declare no competing financial interests.

Methods

Coastal change data sets collected between 1979 and 2012 with a minimum of five consecutive years of at least semi-annual survey frequency were compiled from 48 individual locations, representing 16 study sites throughout the Pacific Ocean basin, including sites in New Zealand, Australia (New South Wales and Queensland), Japan, Central Pacific (Hawaii, USA), Pacific Northwest (British Columbia, Canada and Washington/Oregon, USA) and California (USA) (Supplementary Table 2). Representative shoreline proxies were extracted from a variety of data sources (for example, cross-shore profiles, 3D surface maps) and assimilated by sub-region to develop a time series of shoreline evolution. From this time series, shoreline change metrics were calculated, such as mean annual position and maximum annual change (shoreline advance/retreat) for potential correlation with wave and water level conditions, and climate indices. The annual shoreline erosion anomaly for each site was calculated as:

$$s = \frac{\bar{y}_{\min} - y_{\min}}{|\bar{y}_{\min}|}$$

where $y_{\min}$ is the minimum annual shoreline position and $\bar{y}_{\min}$ represents the mean of this quantity over the entire record. Hence, positive values of the anomaly, s, correspond to the percentage of the erosion anomaly larger than the mean.

For each of the 16 study sites, co-located wave (that is, significant wave height, mean wave period and mean wave direction) and water level data (that is, hourly observed and predicted) were identified to assess intra- and interannual variability in wave forcing and water level anomalies from 1979 to 2012. ECMWF ERA-Interim reanalysis[24] was used to provide 6-h wave climate data at $1.5^\circ \times 1.5^\circ$ grid cell resolution. Wave height, period and direction data from wave buoys within the study area were found to be significantly correlated with adjacent ERA-Interim data—for example, significant wave-height R-values range from 0.74–0.94, and root-mean-square 0.4 to 0.77 m (ref. 40). Wave directions with especially low correlations were removed for final analysis (except for the NZ regions without co-located wave buoy data for accuracy assessment). US wave buoy data came from the National Data Buoy Center (NDBC) whereas international data was sourced from local government agencies. Therefore, to maintain consistency between regions, and extend the record further back in time, ERA-Interim data was used in lieu of *in situ* wave buoys. Wave energy flux, F, was calculated using:

$$F = \frac{\rho g^2 H_s^2 T}{64\pi}$$

where $\rho = 1{,}025\,\mathrm{kg\,m^{-3}}$ is the density of seawater, g is the gravitational constant, H_s is the significant wave height, and T is the wave period. Wave directional anomaly was calculated as the number of degrees clockwise or anticlockwise of the mean direction. Water level data were gathered from nearby tide stations, which are usually located in semi-enclosed harbours and sheltered from waves.

All data were binned into wave-year (1 November–31 October) averages to account for both northern (DJF, 1 December–28 February) and southern hemisphere winters (JJA, 1 June–31 August). A summary of the annual wave climate for each region is shown in Supplementary Fig. 2.

Covering the same time period from 1979 to 2012, 12 climate indices relevant to the Pacific Ocean basin and regional climate (Supplementary Fig. 1 and Supplementary Table 1) were gathered from a variety of sources: Pacific Decadal Oscillation (PDO), Interdecadal Pacific Oscillation (IPO), El Niño Modoki Index (EMI), Multivariate ENSO Index (MEI), Oceanic Niño Index (ONI), Southern Oscillation Index (SOI), Southern Annular Mode (SAM), Arctic Oscillation (AO), Northern Oscillation Index (NOI), North Pacific Gyre Oscillation (NPGO), North Pacific Index (NPI), Pacific North American (PNA). Climate indices were yearly and DJF averaged to the same dates as all other data. The five highest and five lowest values from each index averaged over yearly and DJF periods were used to identify relationships between wave energy flux, direction, water level and shoreline change (Supplementary Table 3).

Code availability. The codes and data used to generate the results for this project are available upon request from the corresponding author.

References

40. Harley, M. D., Barnard, P. L. & Turner, I. L. *Coastal Sediments 2015: The Proceedings of the Coastal Sediments 2015* (World Scientific, 2015).